

# Processing, Characterization and Fretting Wear of Zinc Oxide and Silver Nanoparticles Reinforced Ultra High Molecular Weight Polyethylene Biopolymer Nanocomposite

FAHAD ALAM,<sup>1</sup> ANIL KUMAR,<sup>1</sup> ANUP KUMAR PATEL,<sup>1</sup>  
RAJEEV K. SHARMA,<sup>1</sup> and KANTESH BALANI<sup>1,2</sup>

1.—Biomaterials Processing and Characterization Laboratory & Surface and Tribology Laboratory, Materials Science and Engineering, Indian Institute of Technology Kanpur, Kanpur 208016, India. 2.—e-mail: kbalani@iitk.ac.in

Ultra-high molecular weight polyethylene (UHMWPE) is the most widely used biopolymer for articulating surfaces, such as an acetabular cup liner interfacing with a metal/ceramic femoral head. However, the formation of wear debris leads to the aseptic loosening of implants. Thus, in order to improve the life span via enhancing the fretting wear resistance, UHMWPE is reinforced with ZnO/Ag nanoparticles. It is envisaged that the ZnO/Ag addition will also exhibit antibacterial properties. In the current study, the synergetic effect of the reinforcement of ZnO/Ag nanoparticles (0–3 wt.% combinations) on the fretting wear behavior of a UHMWPE matrix is assessed. The phase characterization of compression-molded UHMWPE-Ag-ZnO biopolymer nanocomposites has elicited the retention of starting phases. All samples were processed at >98% density using compression molding. Silver and ZnO reinforcement showed enhanced hardness ~20.4% for U3A and 42.0% for U3Z. Fretting wear performance was evaluated at varying loads (5–15 N), keeping in mind the weight at different joints, with constant frequency (5 Hz) as well as amplitude of oscillation (100  $\mu\text{m}$ ). Laser surface profilometry showed change of wear volume from  $8.6 \times 10^{-5} \text{ mm}^3$  for neat polymer to  $5.8 \times 10^{-5} \text{ mm}^3$  with 1 wt.% Ag + 1 wt.% ZnO reinforcement (at 15 N load). Consequently, the mechanics of resistance offered by Ag and ZnO is delineated in the UHMWPE matrix. Further, *S. aureus* viability reduction is ~28.7% in cases with 1 wt.% Ag addition, ~42.5% with 1 wt.% ZnO addition, but synergistically increase to ~58.6% and 47.1% when each of Ag and ZnO is added with 1 wt.% and 3 wt.%, respectively (when compared to that of the UHMWPE control sample). Increased wear resistance and superior bioactivity and enhanced anti-bacterial properties of 1 wt.% Ag + 1 wt.% ZnO and 3 wt.% Ag + 3 wt.% ZnO shows the potential use of ZnO-Ag-UHMWPE biopolymer composites as an articulating surface.

## INTRODUCTION

Fretting is an oscillatory motion, normally tangential, of small amplitude, ~100  $\mu\text{m}$ , which causes the release of the smaller particles as wear debris from the surface of the mating materials.<sup>1,2</sup> Once the smaller particles are released (as wear debris) from the surface of the implant materials, they remain in contact with the cup liner and head due to constricted motion, which results in the loss of

clearance of the total joints and causes implant loosening.<sup>3</sup> It can also cause jamming of the joints when wear debris are strongly held in contact.<sup>4</sup> Fretting wear is one of the most common factors for the failure of total joint replacements.<sup>3</sup> Fretting wear induces osteolysis, which is an active resorption of bone matrix by osteoclasts that occur at the proximity of prosthesis. Osteolysis either causes an immunological response or changes in the bone's structural load.<sup>5</sup> Implant-induced osteolysis is

caused by the adverse cellular response to phagocytosable particulate wear and wear debris.<sup>6</sup>

Various metallic and ceramic particles (such as Ti, Al<sub>2</sub>O<sub>3</sub>, CoCrMo, ZrO<sub>2</sub>, hydroxyapatite and TiO<sub>2</sub>) are used as reinforcements to improve the wear resistance of the implant materials.<sup>7–13</sup> There are a few studies based on blending of ultra-high molecular weight polyethylene (UHMWPE) with high density polyethylene (HDPE) to change the mechanism of wear.<sup>14,15</sup> Some of the reinforcements provide better wear properties at the cost of biological properties, whereas some provide a superior biological response at the cost of mechanical properties.<sup>16,17</sup> Biomaterial-associated infection (BAI) is one of the most challenging issues that causes failure of implants<sup>18</sup> and much research is being carried out to improve the anti-bacterial properties of the implants to avoid BAI. Silver (Ag) and ZnO are well known for their anti-bacterial properties.<sup>19,20</sup> Hence, we have used them as reinforcements with UHMWPE to improve the anti-bacterial property.

In the present study, an effort has been made to improve the fretting wear as well as anti-bacterial properties of compression-molded UHMWPE<sup>21,22</sup> by reinforcing Ag nanoparticles and ZnO microrods. Samples were processed by compression molding and characterized by x-ray diffraction (XRD), Fourier transform infrared spectroscopy (FT-IR), differential scanning calorimetry (DSC) and thermal gravimetric analysis (TGA). Fretting wear tests were performed in order to assess the wear performance and observe the effect of variation in load (5–15 N) on the compression-molded samples of pure UHMWPE and the composites (see Table I for detailed nomenclature and combinations). The objective of the current work is to enhance the bactericidal property of UHMWPE with synergistic ZnO/Ag reinforcements while retaining/enhancing its tribological resistance. By reinforcement of Ag and ZnO in UHMWPE, bioactivity as well as nanomechanical properties are expected to change (i.e. BAI on these biomaterials is expected to decrease). So, an additive effect of Ag and ZnO reinforcement on affecting its antibacterial property and tribological resistance (via fretting) is assessed in UHMWPE-based biopolymeric nanocomposites.

## MATERIALS AND METHODS

### Processing of UHMWPE-Ag-ZnO Biopolymer Composites

UHMWPE medical grade powder (GUR<sup>TM</sup> 1020) (Fig. 1a; average size  $\sim 22 \mu\text{m}$ , density of  $0.93 \text{ g/cm}^3$ ) was supplied by Ticona (Werk Ruhrchemie, Germany). ZnO micro-rods (Fig. 1b; length  $\sim 10 \mu\text{m}$  and diam.  $\sim 2 \mu\text{m}$ ) were prepared by a hydrothermal method,<sup>23</sup> whereas Ag nanoparticles (Fig. 1c;  $\sim 20 \text{ nm}$  and purity 99%) were purchased from Loba Chemie. The polymer and nanoparticles were blended by ball milling (Fritsch Ball Mill P-7, Germany) without balls for 4 h at 300 rpm (pause of 10 min after every 30 min of blending). The distribution and retention of Ag and ZnO on the surface of UHMWPE powder is observed in Fig. 1d. Finally, the blended powders were compression molded (using a SCM-30 compression molding unit; M/s Santec Automation, Delhi) at a pressure of 7.5 MPa and 200°C with a dwell time of 1 h, followed by cooling of the die to room temperature in air. Nine different compositions of UHMWPE (U), UHMWPE + 1% Ag (U1A), UHMWPE + 1% ZnO (U1Z), UHMWPE + 3% Ag (U3A), UHMWPE + 1% ZnO (U3Z), UHMWPE + 1% Ag + 1% ZnO (U1A1Z), UHMWPE + 1% Ag + 3% ZnO (U1A3Z), UHMWPE + 3% Ag + 1% ZnO (U3A1Z) and UHMWPE + 3% Ag + 3% ZnO (U3A3Z) were prepared using two sized dies, i.e. cylindrical pellets ( $\Phi = 12 \text{ mm}$  and  $t = \sim 3 \text{ mm}$ ) for biological study, and square sheets ( $9 \times 9 \text{ cm}$  and  $t = \sim 3 \text{ mm}$ ) for undertaking fretting studies. Surface morphology of a few compression-molded sheets (UHMWPE sheet, U3A, U3Z, and U3A3Z) are shown in Fig. 2.

### Physical and Thermal Characterization

Densification of the sample was calculated using Archimedes principle (with a CITIZEN CX 220 microbalance and ethanol as an immersion medium (density  $\sim 0.789 \text{ g/cm}^3$ )). Weight of all the samples was measured in air and in ethanol, and the difference was used to calculate density and % densification. The density and percentage densification of compression molded pellets is reported in Table I.

**Table I. The compositions, densification and Vickers's hardness for all the samples**

Sample	Sample composition	% densification	Hardness (MPa)
U	UHMWPE	$99.4 \pm 0.3$	$39.2 \pm 2.9$
U1A	UHMWPE + 1 wt.% Ag	$98.9 \pm 0.3$	$43.6 \pm 3.8$
U1Z	UHMWPE + 1 wt.% ZnO	$98.8 \pm 0.2$	$49.4 \pm 2.4$
U1A1Z	UHMWPE + 1 wt.% Ag + 1 wt.% ZnO	$98.3 \pm 0.7$	$50.0 \pm 1.8$
U3A	UHMWPE + 3 wt.% Ag	$99.1 \pm 0.4$	$47.2 \pm 3.3$
U3Z	UHMWPE + 3 wt.% ZnO	$99.8 \pm 0.3$	$55.6 \pm 4.5$
U1A3Z	UHMWPE + 1 wt.% Ag + 3 w % ZnO	$98.5 \pm 0.4$	$51.0 \pm 1.6$
U3A1Z	UHMWPE + 3 wt.% Ag + 1 wt.% ZnO	$98.7 \pm 0.5$	$50.8 \pm 2.1$
U3A3Z	UHMWPE + 3 wt.% Ag + 3 wt.% ZnO	$99.1 \pm 0.3$	$53.4 \pm 3.4$

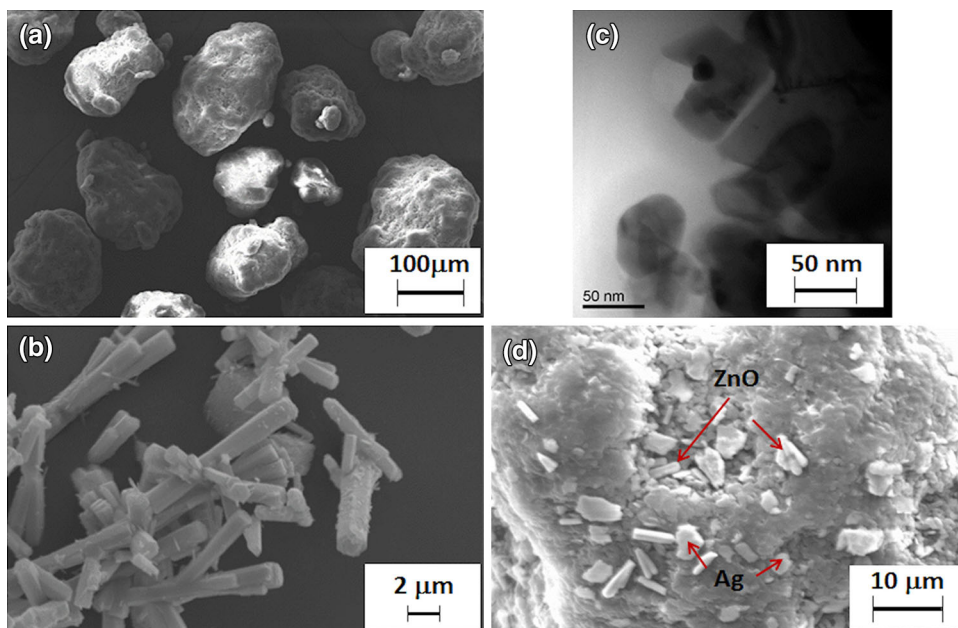


Fig. 1. Images showing morphology and size of starting powders: (a) UHMWPE particles, (b) ZnO rods, (c) Ag nanoparticles (using bright field TEM), and (d) composite powder showing the presence of ZnO and Ag on the surface of UHMWPE polymer particles.

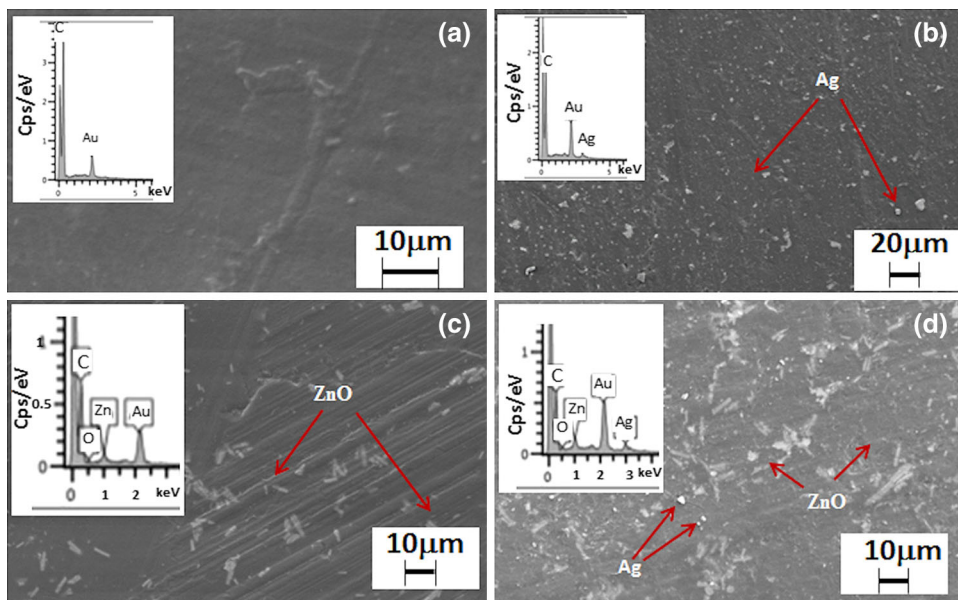


Fig. 2. Surface morphology of compression molded sheets: (a) U, (b) U3A, (c) U3Z, and (d) U3A3Z, composite sheets showing the presence of ZnO and Ag dispersed in the matrix of UHMWPE. Inset of all images are their energy dispersive spectra (EDS).

Melting point and the weight loss of all the starting powders and prepared pellets were measured using differential scanning calorimetry (DSC) and thermal gravimetric analysis (TGA), respectively, using a Perkin Elmer DTA 6000. Temperature scanning range was selected between 40°C and 220°C with a holding time of 2 min at 220°C for DSC and 40–600°C with holding time of 2 min at 600°C for TGA. Nitrogen gas atmosphere was used with heating and cooling rates being 10°C/min.

### Phase and Microstructural Characterization

All the starting powders and the prepared pellets were characterized by x-ray diffraction to identify the phases present in the sample. Cu K- $\alpha$  radiation ( $\lambda = 1.541 \text{ \AA}$ ) operated at 25 kV and 15 mA was used as x-ray source (using a Rich-Seifert 2000D diffractometer) with a scan speed of 2.4°/min, step size of 0.02° with  $2\theta$  ranging from 10° to 80°. Scanning electron microscopy (SEM; Carl Zeiss SUPRA 40VP, Germany) operated at 20 kV, and transmis-

sion electron microscopy (TEM; FEI UT 20) with an accelerating voltage of 200 kV, were performed to characterize and study the particle size.

### Surface Energy Calculation

For the calculation of surface energy, the contact angle on the sample were measured by a computer-controlled goniometer system (Dataphysics Contact Angle System OCA) performing sessile drop with one polar (water) and three non-polar (chloroform, xylene and toluene) liquids. Surface energy plays a critical role on dictating the protein adsorption and consequent cellular response on the material surfaces, thus wettability studies were performed to assess them. Then, the polar component and dispersion components were calculated using Owens–Wendt–Rabel–Kaelble geometric mean equations as below:<sup>24</sup>

$$\sigma_s = \sigma_{s1} + \sigma_1 \cdot \cos \theta \quad (1)$$

$$\sigma_1 = \sigma_1^d + \sigma_1^p \quad (2)$$

$$\sigma_s = \sigma_s^d + \sigma_s^p \quad (3)$$

$$\sigma_{s1} = \sigma_s + \sigma_1 - \left( 2\sqrt{\sigma_s^d \cdot \sigma_1^d} + \sqrt{\sigma_s^p \cdot \sigma_1^p} \right) \quad (4)$$

$$\frac{1 + \cos \theta}{2} \cdot \frac{\sigma_1}{\sqrt{\sigma_1^d}} = \sqrt{\sigma_s^p} \sqrt{\frac{\sigma_1^p}{\sigma_1^d}} + \sqrt{\sigma_s^d} \quad (5)$$

where,  $\sigma_{s1}$  is the interfacial tension between liquid and solid,  $\sigma_s$  is the surface energy of the solid surface,  $\sigma_1$  is the surface tension of the liquid,  $\sigma_s^d$  is the dispersion component of the solid,  $\sigma_s^p$  the polar components of the solid, and  $\theta$  is the contact angle between the solid and the liquid.

### Mechanical Testing and Fretting Wear of ZnO and Ag Reinforced UHMWPE

Bulk hardness of the processed sample was measured using Vickers's hardness tester (BAREISS-V-TEST; Bareiss Prüfgerätebau, Germany) by applying 100-g load with a dwell time of 10 s. The diagonals of the Vickers indents were then measured using an optical microscope. A total of five to six measurements were taken and their average value is reported as the hardness.

Fretting was done using a fretting wear tester (DUCOM TR281 M; Reciprocating Wear and Friction Tester; Bangalore, India) by employing a ball-on-flat-type configuration (see Fig. 3) with the variation of load from 5 N to 15 N. The frequency and

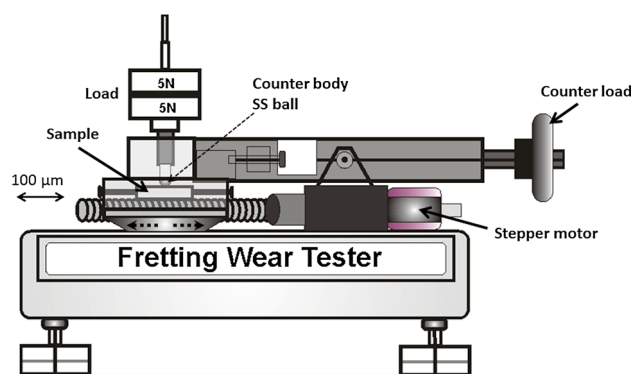


Fig. 3. Schematic of the fretting wear tester.

the amplitude of the motion were kept constant (5 Hz and 100  $\mu\text{m}$ ) for all samples.

### Bioactivity Immersion Test

All samples were tested for *in vitro* bioactivity test by their immersion in the simulated body fluid (SBF) and Dulbecco's Modified Eagle's Medium (DMEM) media purchased from Sigma-Aldrich. Samples were immersed in both SBF and DMEM in an incubator at 37°C for 48 h, then dried and examined under SEM to observe the growth of the apatite layer on the surface of the samples. These grown apatite layers were further characterized by XRD to confirm the presence of the apatite layer, and the quantified apatite percentage is compared along with neat UHMWPE (U).

### Anti-bacterial Test

#### Bacterial Viability Assay (MTT)

All the samples were incubated with *S. aureus* (ATCC # 25923) for 4 h at 37°C in the presence of LB (Luria Broth) media. For this study, only one type of bacteria (Gram-positive) was selected, so it must be noted that Gram-negative bacteria may not mimic such a response. After incubation, all samples were washed thoroughly to remove the slackly attached bacteria on the sample surface and then all samples were incubated with MTT [3(4,5-dimethylthiazol-2-yl)—2,5-diphenyl tetrazolium bromide] for 1 h at room temperature. The formed insoluble formazan crystals were dissolved in 200 mL dimethyl sulfoxide and then absorbance (optical density) of the produced violet color solutions were measured at 540 nm wavelength. The U sample was taken as the negative control, as no additive was incorporated which can restrict the growth of bacteria in this sample. Student's *t* test was performed to check the statistical significance among mean values with a confidence limit of > 95% ( $p < 0.05$ ).

#### Adhesion Assay

For the adhesion and morphological study of *S. aureus* bacteria, all the samples were incubated for 8 h at 37°C in the presence of LB media. Samples were fixed

by 3.7% glutaraldehyde for 20 min and 0.1 M sucrose solution was added to each well for 10 min, and then washed twice with ethanol series (30%, 50%, 70%, and 90%) for 10 min each. Finally, all samples were dried to critical point by HMDS for just a few seconds and gold-coated prior to SEM imaging for observing the morphology of the adhered bacteria.

## RESULTS AND DISCUSSION

### Physical and Mechanical Characterization of Compression-Molded UHMWPE-ZnO-Ag Biopolymer Composite

The ZnO- and Ag-reinforced compression-molded UHMWPE samples are shown in Fig. 4. The density of the prepared pellets was calculated by Archimedes principle and it was observed that the densification of all the samples was more than 98% (Table I). Further, Vickers hardness was observed to increase with increase of the reinforcement content (Table I), i.e. 39.2 MPa for U to 55.6 MPa for U3Z composite samples. Enhanced hardness of the composites indicate probable enhancement of the tribological resistance of the biopolymeric nanocomposites (required for materials used as articulating surfaces).

### Phase Characterization of UHMWPE-ZnO-Ag Samples

Figure 5a, b show the XRD spectra of the starting powders and prepared pellets. From these patterns, it can be observed that no new phase has formed and

all the starting phases are retained after compression molding. For the Ag nanoparticles (NPs), the peaks were observed at  $2\theta$  values of  $38.2^\circ$ ,  $44.3^\circ$  and  $64.7^\circ$ <sup>25</sup> and for the ZnO, peaks were observed at  $2\theta$  values of  $31.8^\circ$  and  $36.2^\circ$ ,<sup>26</sup> which were absent in the neat polymer, indicating the retention of Ag and ZnO phases in the compression-molded samples. Peaks at  $2\theta$  values of  $10.1^\circ$ ,  $22.0^\circ$  and  $24.1^\circ$  are the characteristic peaks of UHMWPE.<sup>27</sup>

### Thermal Analysis

From the thermal analysis (Fig. 6a; differential scanning calorimetry), it was observed that the melting point of starting powders is  $\sim 140^\circ\text{C}$ , and did not change much with the reinforcements. The estimation of melting point allows the adopting of appropriate temperatures for processing biopolymeric nanocomposites. In order to accommodate the thermal gradient in the die, the compression-molding temperature was kept at  $200^\circ\text{C}$ . From the thermogravimetric analysis of the compression-molded pellets (Fig. 6b), it can be observed that the addition of both Ag and ZnO results in a marginally lower weight loss. Finally, the crystallinity of the processed samples was measured and compared with that of the starting powders (crystallinity of  $\sim 41.5\text{--}48.8\%$ ). A decrease in crystallinity ( $\sim 19.2\text{--}28.3\%$ ) was observed after compression molding (Table II). Enhanced degrees of crystallization also enhance hardness (thus tribological resistance) and is useful in restricting the degradation of the polymer under biological conditions.

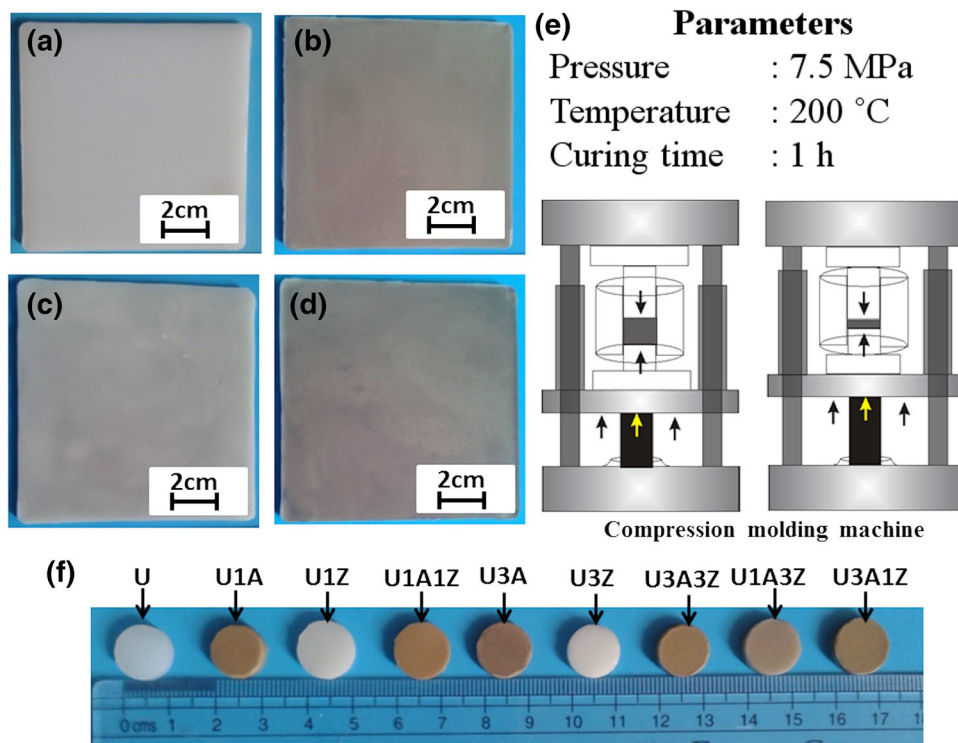


Fig. 4. Compression-molded UHMWPE-ZnO-Ag sheets and pellets along with the processing conditions (a) U, (B) U3A, (C) U3Z, (d) U3A3Z sheets, (e) schematic of compression molding, and (f) compression molded pellets.

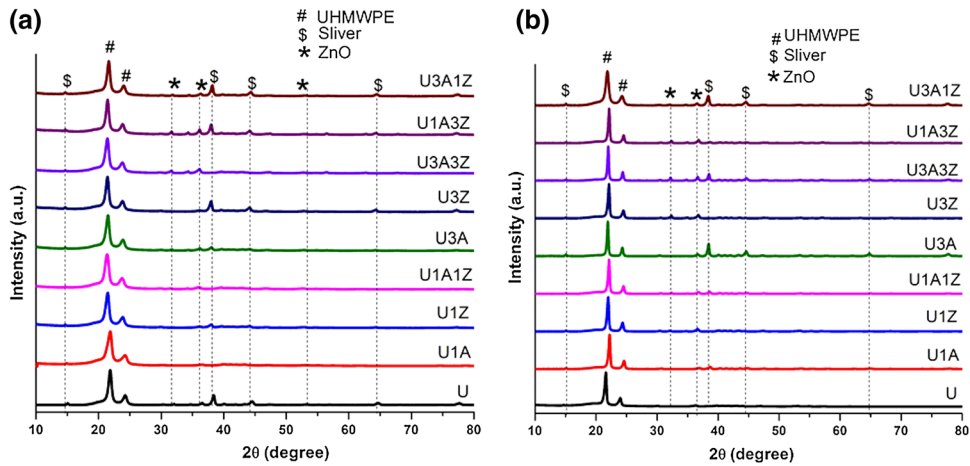


Fig. 5. XRD spectrum of (a) starting powders and (b) compression-molded pellets.

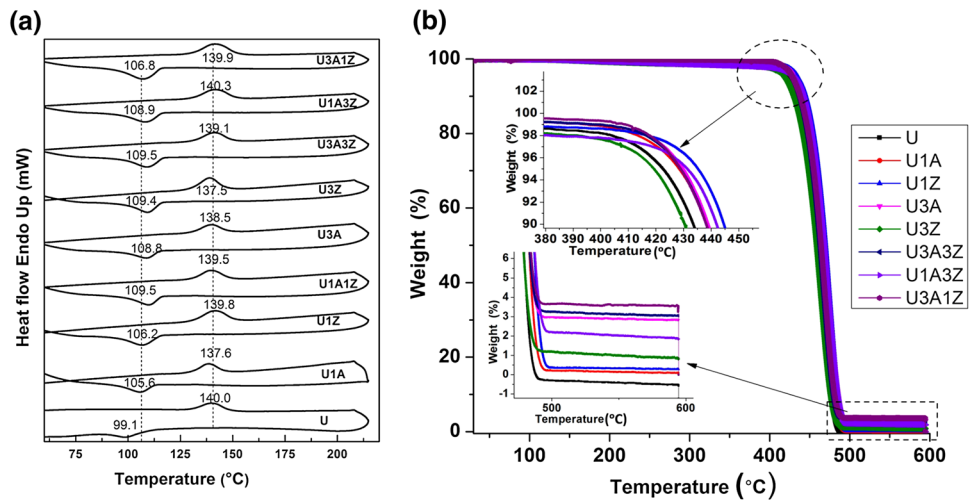


Fig. 6. (a) DSC profile of the starting powders in which dotted lines at around 100 °C and at around 140 °C are marked to compare the peak temperature of both the heating cycle and the cooling cycle. (b) TGA profile represents the profile of wt.% of all the samples. Inset is the magnified image the neck region of weight loss after TGA for all samples.

**Table II. Melting temperature and % crystallization of the starting, with percent crystallization of the compression-molded pellets presented for comparison**

Sample	Onset temp. (°C)	Peak temp. (°C)	End temp. (°C)	Delta H (J/g)	% crystallization of powder	% crystallization of pellets
U	130.4	140.0	148.0	120.6	41.5	29.3
U1A	129.9	137.6	144.8	123.8	42.6	28.6
U1Z	129.8	139.8	149.2	121.7	41.9	28.5
U1A1Z	129.8	139.5	147.7	121.9	42.0	19.2
U3A	129.4	138.5	145.9	129.9	44.7	27.1
U3Z	128.7	137.5	145.4	132.7	45.7	23.1
U1A3Z	129.6	140.3	149.8	121.1	41.7	21.1
U3A1Z	129.4	139.9	151.0	123.5	42.5	24.5
U3A3Z	130.9	139.1	148.0	128.6	48.8	27.1

**Surface Energy of Compression Molded UHMWPE-ZnO-Ag Biopolymeric Nanocomposite**

Contact angles with water for all the samples are represented in Fig. 7 and the results of calculated surface energy are shown in Table III. It can be seen that the addition of Ag NPs decreased the surface energy from 29.03 mN/m to 28.31 mN/m, whereas the addition of ZnO rods resulted in an increase from 29.03 mN/m to 32.31 mN/m, and also the polar components increased from 5.6 mN/m to 11.02 mN/m by adding Ag/ZnO. Dispersion components are maximum and polar component are minimum when both Ag and ZnO are reinforced (Table III). Since the newly developed UHMWPE-Ag-ZnO biopolymer composites are expected to be cytocompatible, a higher dispersion component confirms this (Table III).

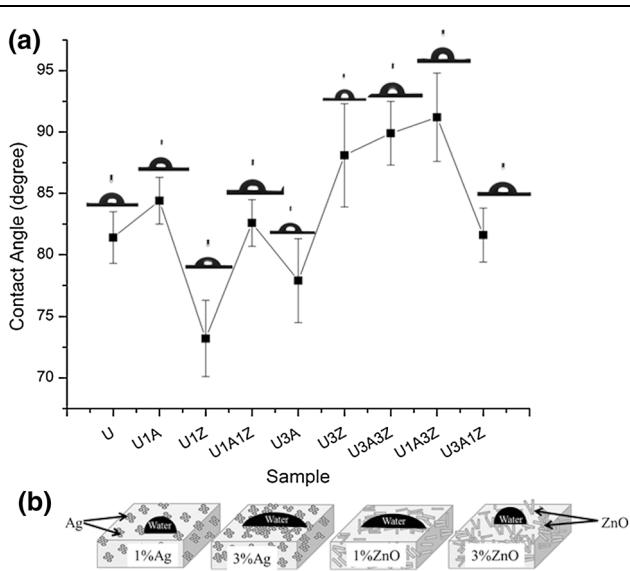


Fig. 7. (a) The contact angles of all the samples are plotted with respect to their composition. (b) Schematic showing change in contact angles with addition of Ag and ZnO.

**Fretting Wear Analysis**

Reinforcement of Ag and ZnO is anticipated to render antibacterial property (as confirmed in later section), such an addition should not deleteriously affect the tribological property of the acetabular cup liner. Thus, fretting wear has been performed to assess the wear when the testing load was varied from 5 N to 15 N and wear volume were calculated using a laser surface profilometer (LSP) (Perthometer PGK 120, Mahr, Germany). In this non-destructive profiling technique (LSP), an infra-red laser beam of wavelength  $\lambda = 780$  nm formed into a circular beam of  $2 \mu\text{m}$  diameter was used to trace the dimensions of the wear scar. From the results, it was observed that silver NPs help to decrease the wear volume (see Table IV), whereas ZnO rods lead to increases in the wear volume. The least wear rate (of  $2.5 \times 10^{-6} \text{ mm}^3/\text{N.m}$ ) is obtained for U3A. However, the synergy of Ag and ZnO comes into play and a lower wear volume is obtained (from  $8.6 \times 10^{-5} \text{ mm}^3$  for U to  $5.8 \times 10^{-5} \text{ mm}^3$  with U1A1Z, at 15 N load), while achieving a marginally lower wear rate (Table IV). Wear rate was calculated using the following equation and shown in Table IV.

Wear rate

$$= \frac{\text{Wear volume (mm}^3\text{)}}{\text{Load (N)} \times \text{number of cycles} \times \text{stroke length (\mu m)}}$$

The change in the coefficient of friction of UHMWPE-ZnO-Ag samples at varying loads is shown in Fig. 8a. Further, the area under the hysteresis loop for all the compression-molded samples was analyzed at different loads (5–15 N) (Fig. 8b–d). The area of the fretting hysteresis can be calculated by the following equation:<sup>28</sup>

$$A = \int Ft(D)ds \tag{6}$$

where, ds is the displacement amplitude.

**Table III. Surface energy, polar fraction and dispersion fraction of compression-molded UHMWPE-Ag-ZnO biopolymeric nanocomposites**

Sample	Surface energy (mN/m)	Polar part (mN/m)	Dispersion part (mN/m)	Polar fraction	Dispersion fraction
U	29.03	5.67	23.36	0.20	0.80
U1A	28.31	4.10	24.21	0.14	0.86
U1Z	32.31	11.02	21.38	0.34	0.66
U1A1Z	28.78	4.98	23.80	0.17	0.83
U3A	28.49	4.30	24.19	0.15	0.85
U3Z	30.05	8.80	21.25	0.29	0.71
U1A3Z	29.41	4.27	25.14	0.15	0.85
U3A1Z	29.41	5.29	24.12	0.18	0.82
U3A3Z	28.00	2.97	25.03	0.10	0.90

**Table IV. Wear volume and wear rate calculated from laser surface profiling of compression-molded UHMWPE-ZnO-Ag samples after fretting at different loads**

Samples	Load 5 N		Load 10 N		Load 15 N	
	Wear volume (mm <sup>3</sup> )	Wear rate (mm <sup>3</sup> /N m)	Wear volume (mm <sup>3</sup> )	Wear rate (mm <sup>3</sup> /N m)	Wear volume (mm <sup>3</sup> )	Wear rate (mm <sup>3</sup> /N m)
U	$8.7 \pm 0.2 \times 10^{-6}$	$1.74 \times 10^{-6}$	$4.9 \pm 0.7 \times 10^{-5}$	$4.9 \times 10^{-6}$	$8.6 \pm 0.4 \times 10^{-5}$	$5.7 \times 10^{-6}$
U1A	$5.4 \pm 0.2 \times 10^{-6}$	$1.08 \times 10^{-6}$	$2.7 \pm 0.2 \times 10^{-5}$	$2.7 \times 10^{-6}$	$5.3 \pm 0.4 \times 10^{-5}$	$3.5 \times 10^{-6}$
U1Z	$6.2 \pm 0.3 \times 10^{-6}$	$1.24 \times 10^{-6}$	$3.0 \pm 0.3 \times 10^{-5}$	$3.0 \times 10^{-6}$	$6.8 \pm 0.2 \times 10^{-5}$	$4.5 \times 10^{-6}$
U1A1Z	$6.5 \pm 0.6 \times 10^{-6}$	$1.3 \times 10^{-6}$	$3.2 \pm 0.2 \times 10^{-5}$	$4.2 \times 10^{-6}$	$5.8 \pm 0.2 \times 10^{-5}$	$3.8 \times 10^{-6}$
U3A	$4.8 \pm 0.3 \times 10^{-6}$	$9.6 \times 10^{-7}$	$2.2 \pm 0.3 \times 10^{-5}$	$3.2 \times 10^{-6}$	$3.8 \pm 0.6 \times 10^{-5}$	$2.5 \times 10^{-6}$
U3Z	$7.7 \pm 0.4 \times 10^{-6}$	$1.54 \times 10^{-6}$	$5.2 \pm 0.5 \times 10^{-5}$	$5.2 \times 10^{-6}$	$8.9 \pm 0.3 \times 10^{-5}$	$5.9 \times 10^{-6}$
U1A3Z	$9.3 \pm 0.6 \times 10^{-6}$	$1.86 \times 10^{-6}$	$6.1 \pm 0.9 \times 10^{-5}$	$6.1 \times 10^{-6}$	$8.5 \pm 0.6 \times 10^{-5}$	$5.3 \times 10^{-6}$
U3A1Z	$8.8 \pm 0.6 \times 10^{-6}$	$1.76 \times 10^{-6}$	$3.8 \pm 1.0 \times 10^{-5}$	$3.8 \times 10^{-6}$	$5.3 \pm 0.8 \times 10^{-5}$	$3.5 \times 10^{-6}$
U3A3Z	$8.7 \pm 0.3 \times 10^{-6}$	$1.74 \times 10^{-6}$	$5.1 \pm 0.4 \times 10^{-5}$	$5.1 \times 10^{-6}$	$8.1 \pm 0.7 \times 10^{-5}$	$5.4 \times 10^{-6}$

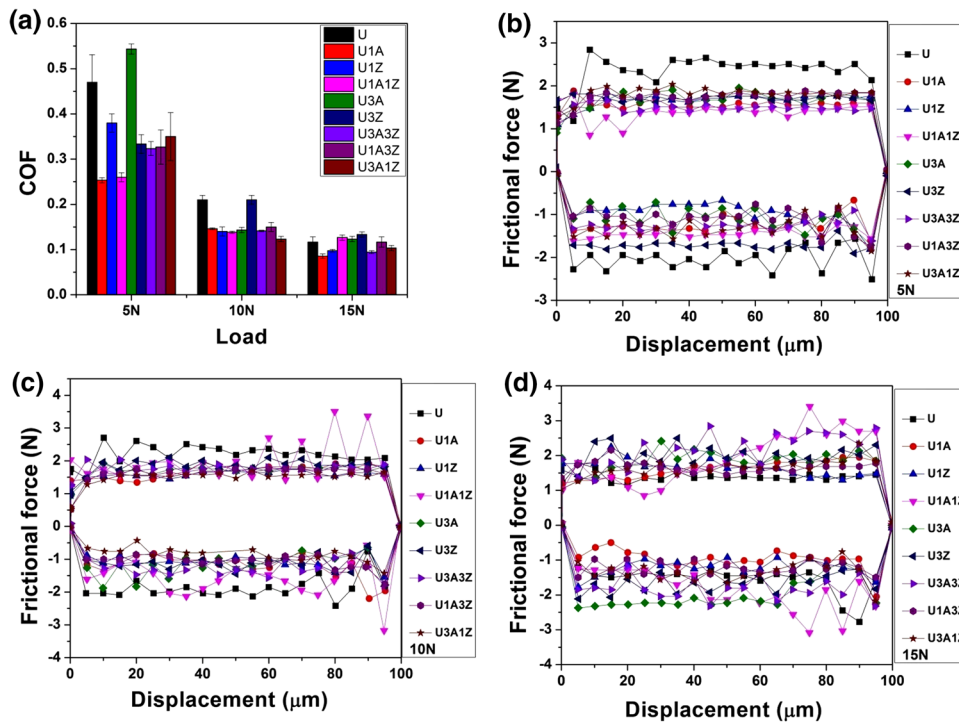


Fig. 8. (a) Coefficients of friction of compression-molded UHMWPE-ZnO-Ag samples with varying load, and friction hysteresis of all samples at (b) 5 N, (c) 10 N, and (d) 15 N showing the change in the energy dissipation with the addition of Ag and ZnO particles. The x-axis (in b–d) shows the fretting amplitude of 100 μm, and its corresponding frictional force (in N) is presented on the y-axis.

The total area enclosed by the friction hysteresis represents the energy dissipated during each fretting cycle. It was found that the energy dissipation, as expected, increased with increases in the normal load from 5 N to 15 N (Table V). Figure 9 shows the imaging of the wear scar by optical microscopy (Fig. 9a) for four samples, viz. U, U3A, U3Z and U1A3Z. The wear volume was calculated using LSP (Table IV) and the corresponding 3D image is represented in Fig. 9b.

### Bioactivity of ZnO- and Ag-Reinforced UHMWPE Biopolymer Composites

After assessing the tribological resistance offered by the UHMWPE-Ag-ZnO biopolymeric nanocomposites, it is essential to ensure that the system remains cytocompatible.<sup>29,30</sup> The precipitation of apatite, both under immersion in SBF (Fig. 10) and DMEM (Fig. 11) is clearly evident via phase characterization (Figs. 10a and 11a) and electron mi-



croscopy images (Figs. 10b–d and 11b–d). From the images, it is evident that ZnO helps to enhance the *in vitro* bioactivity when immersed in either SBF or DMEM. Thinner dendritic apatite morphology is observed under SBF immersion (Fig. 10b–d), whereas thicker apatite precipitation is observed when the immersion media is DMEM (Fig. 11b–d). Apparently, the extent of apatite precipitation in the Ag-reinforced samples is similar to that of UHMWPE (Table VI), but the apatite fraction of the ZnO-reinforced samples is higher than that of neat UHMWPE (Table VI), confirming the enhanced bioactivity of the UHMWPE-ZnO biopolymer composites when compared to their counterpart

**Table V. Area of friction hysteresis at different loads for compression-molded UHMWPE-Ag-ZnO samples**

Sample	Area under hysteresis loop ( $\mu\text{m}^2$ )		
	5 N	10 N	15 N
U	283	395	425
U1A	251	279	307
U1Z	276	296	327
U1A1Z	272	345	367
U3A	270	299	332
U3Z	253	290	329
U1A3Z	248	260	276
U3A1Z	228	288	304
U3A3Z	263	293	384

UHMWPE or Ag-reinforced UHMWPE biopolymeric composites. It may be noted that higher polar fraction in U3Z (Table III) resulted in enhanced apatite precipitation, whereas a higher dispersion fraction in U1A, U3A and U3A1Z) reflects a lower apatite precipitation on the sample surface (Table VI). Hence, in order to optimize the tribological resistance and maintain cytocompatibility, a synergistic combination of Ag-ZnO reinforcement in the UHMWPE matrix is necessary. Further, the purpose of rendering the bactericidal property with Ag and ZnO addition must also be achieved, which is presented in the following section.

### Anti-bacterial Test

To evaluate the bactericidal effect of silver and ZnO, *S. aureus* bacteria were grown on all the UHMWPE-Ag-ZnO biopolymeric nanocomposites (keeping UHMWPE as a negative control) for 8 h in static culture conditions. Figure 12 represents the SEM micrograph of the morphology and the colonies present on the surface of the sample. Figure 12a reveals the highest bacterial density of *S. aureus* in U, whereas the surface of U3A and U3Z shows comparatively less bacterial density (Fig. 12b and c, respectively). It must also be noticed that the colony size is much bigger (running into tens of  $\mu\text{m}$ ; Fig. 12a) when compared to that when Ag or Zn is added (a few  $\mu\text{m}$ ; Fig. 12b and c). The least density of bacteria is observed in both U1A1Z and U3A3Z (Fig. 13), and a representative image of bacteria on

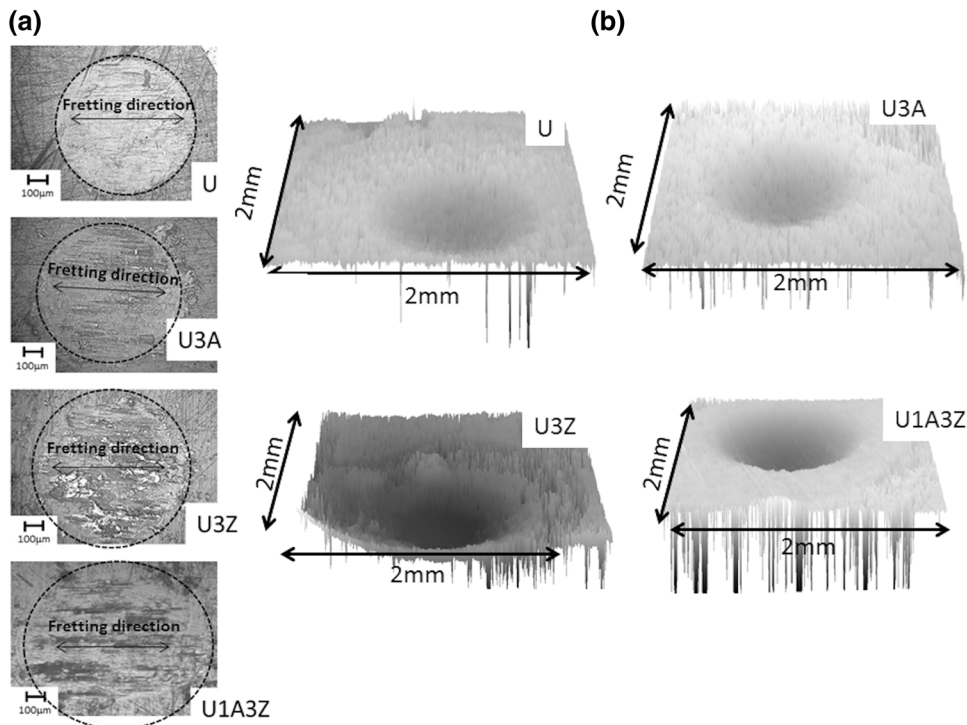


**Fig. 9.** Fretting scars (of U, U3A, U3Z, and U1A3Z) taken by: (a) optical microscopy, (b) laser profilometry (Z axis heights are the same for all), for U, U3A, U3Z and U1A3Z, respectively.

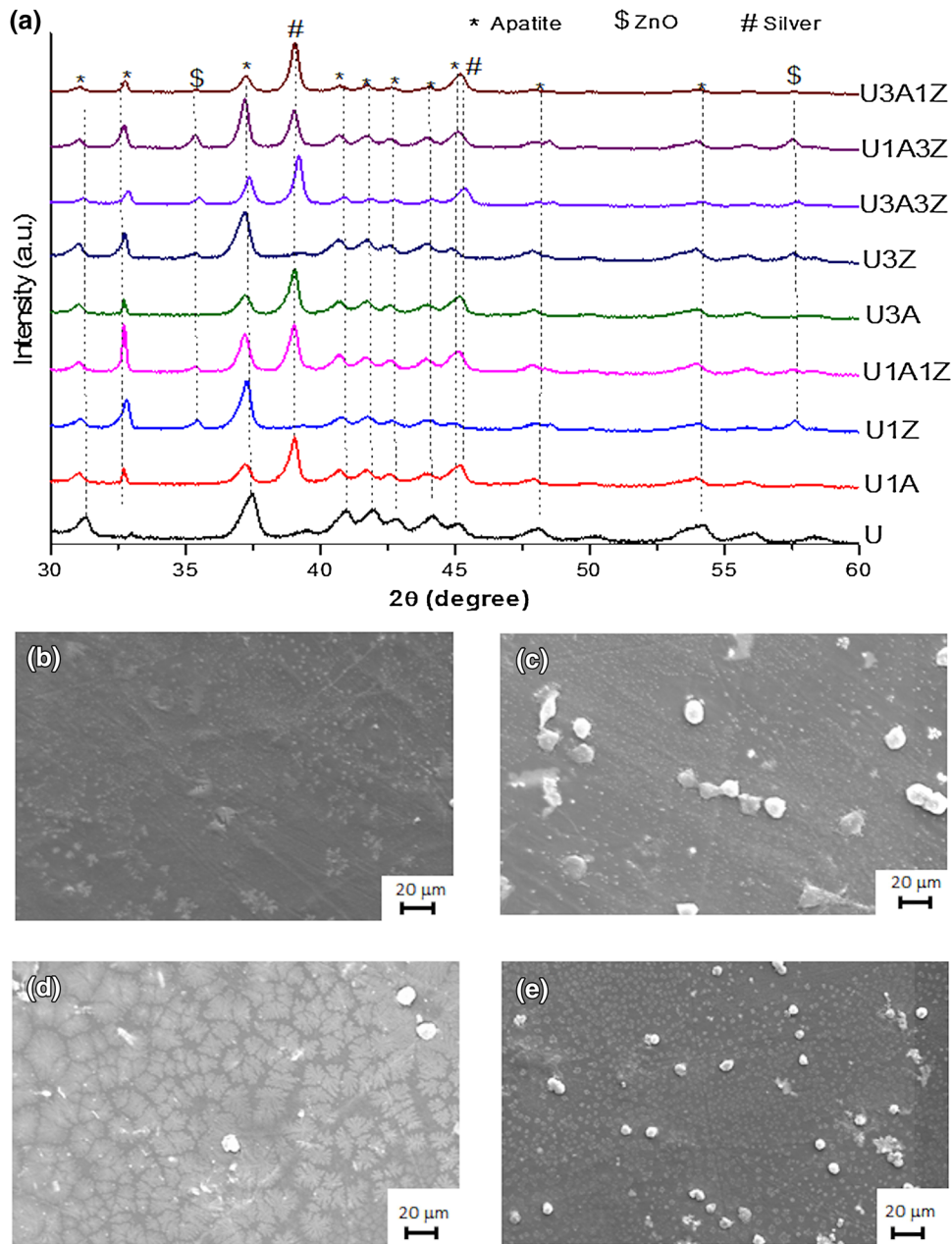


Fig. 10. (a) x-ray diffraction of UHMWPE-ZnO-Ag biopolymeric composites after immersion in SBF showing the presence of apatite. SEM images of the apatite grown after immersion in SBF on the samples: (b) U, (c) U3A, (d) U3Z, and (e) U3A3Z.

U3A3Z composites is shown as Fig. 12d. Apart from a lower bacterial count, clearly the synergistic effect of silver and ZnO on breaking the colony into a small size (i.e. observation of isolated bacteria and not a colony) is also evident.

The analysis of absorbance values shows that *S. aureus* viability reduction is ~28.7% in case of U1A and reduces to ~42.5% in U1Z when compared to that of control (U). However, such viability reduction is ~58.6% in the case of U1A1Z and ~47.1% in U3A3Z composite samples when compared to that of the neat polymer (U) (Fig. 13). It must be realized that the maximum bactericidal property of 42.5% obtained

with U1Z gets enhanced synergistically (to a further reduction), since their decrease is much higher than what was possible earlier with a single reinforcement alone. Had it been an additive effect, then a higher (>58.6% observed for U1A1Z) reduction in bacterial density must be expected in the U3A3Z biopolymer nanocomposite, which is not the case. It is clear that the combined addition of Ag and ZnO in UHMWPE significantly reduces the *S. aureus* growth. This may be attributed to different mechanisms (which is not the scope of the current work) that may be operative (i.e. cell wall rupture with ZnO addition, and DNA-denaturing with Ag addition) in killing the bacteria.<sup>31-33</sup>

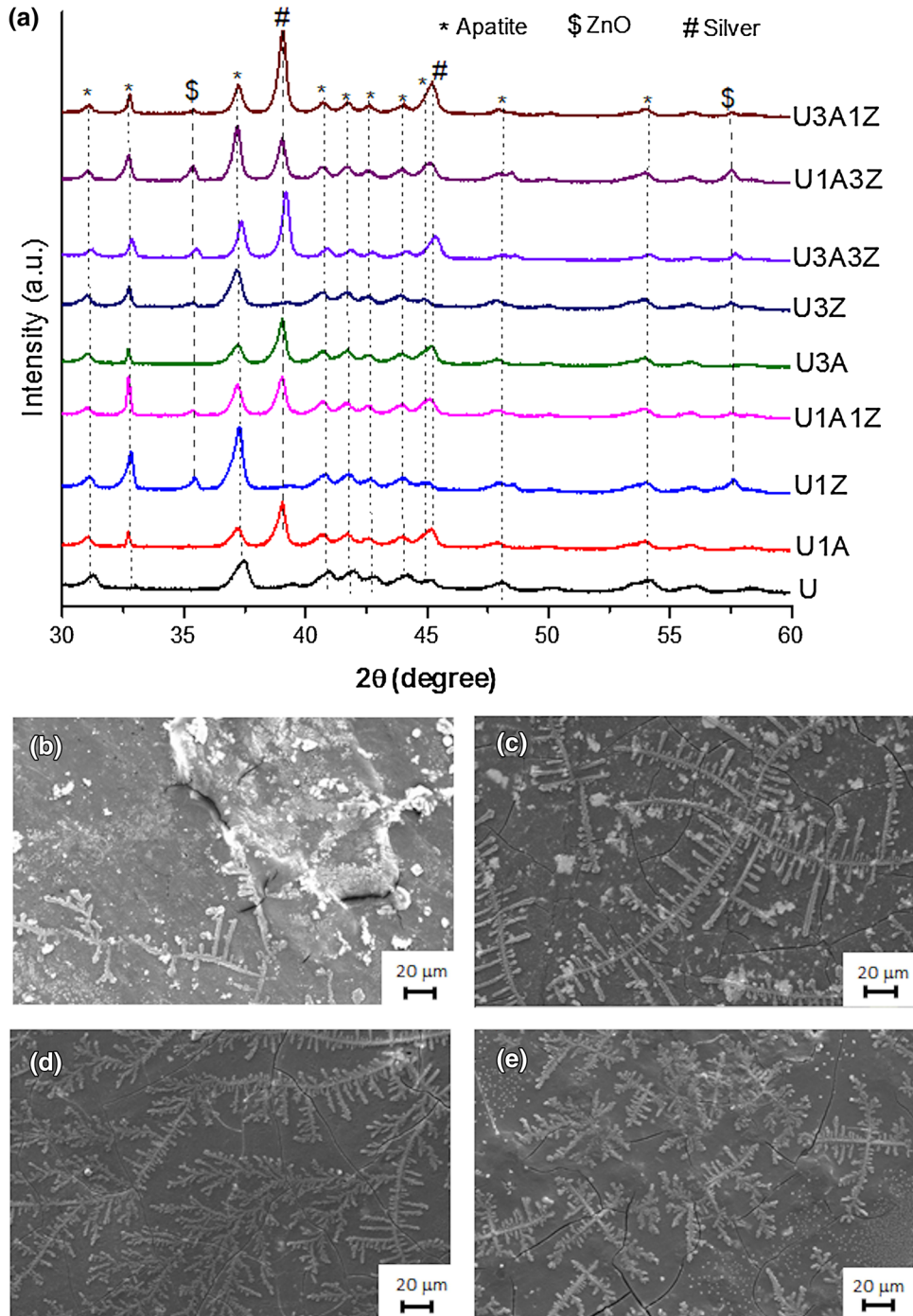


Fig. 11. (a) x-ray diffraction of UHMWPE-ZnO-Ag biopolymeric composites after immersion in DMEM showing the presence of apatite. SEM images of the apatite grown after immersion in DMEM on the samples: (b) U, (c) U3A, (d) U3Z, and (e) U3A3Z.

Figure 14 explains the overall effect of ZnO and Ag NPs reinforcement in the UHMWPE matrix. A schematic (Fig. 14a) shows that increase in concentration of Ag NPs in the composite, water contact angle (WCA) decreased from  $\sim 84^\circ$  (U1Ag) to  $\sim 77^\circ$  (U3A) whereas the increase in ZnO concentration increased WTA from  $\sim 73^\circ$  (U1Z) to  $\sim 88^\circ$  (U3Z) due to orientation of ZnO rods on the surface of the

composite. The EDS map of the U1A3Z composite (Fig. 14b) confirms that the ZnO rods are being pulled out by the counter body, and these pulled out ZnO rods behave like a third body resulting an increase in wear volumes from  $8.6 \times 10^{-5}$  (U) to  $8.9 \times 10^{-5}$  mm<sup>3</sup> (U3Z) at 15 N load which is compensated by Ag  $8.1 \times 10^{-5}$  mm<sup>3</sup> (U3A3Z). Finally, Fig. 14c summarizes that Ag enhances the wear

properties, whereas ZnO increases the bioactivity, so the synergistic effect in the composite U1A1Z and U3A3Z has resulted in an optimum combination of wear resistance and bioactivity (Table VI; Fig. 14c).

From the above observations, it is proposed that ZnO increases the wear volume due to their breakage, whereas Ag NPs help to enhance the wear properties, as shown schematically in Fig. 15. When a counter body comes into contact with the composite's surface, then ZnO rods break and get pulled out (also see Fig. 10b), and these broken parts of the ZnO rods behave as a third body. Thus, the wear mechanism changes to ploughing wear (Fig. 15a), and increases the wear loss. Ag NPs being small in size (~20 nm) come into contact with the counter body and behave like a protective lubricant, and

change the wear mechanism to sliding wear (Fig. 15b) lowering the wear volume, whereas, in the case of UHMWPE-ZnO-Ag composites, the synergistic effect allows the compensation of wear loss caused by the ZnO rods with Ag NPs (Fig. 15c). Thus, a synergistic combination of Ag reinforcement with ZnO is eliciting lower wear rates especially at higher loads, while eliciting apatite precipitation (Table VI) that makes the surface cytocompatible. Thus, both U1A1Z and U3A3Z materials can serve as a potential articulating acetabular cup liner with high wear resistance while exhibiting bactericidal properties.

**Table VI. Quantitative fraction of apatite (from integrated intensity of x-ray diffraction peaks) in different UHMWPE-ZnO-Ag biopolymer composites**

Sample	Fraction of apatite (%) in SBF	Fraction of apatite (%) in DMEM
U	12.5 ± 2.9	16.8 ± 1.7
U1A	11.5 ± 3.4	14.1 ± 2.1
U1Z	21.2 ± 1.6	25.5 ± 3.2
U1A1Z	14.8 ± 1.8	14.6 ± 2.5
U3A	13.1 ± 2.8	15.1 ± 3.3
U3Z	22.5 ± 3.3	31.5 ± 1.5
U1A3Z	17.3 ± 1.1	18.7 ± 2.5
U3A1Z	16.4 ± 2.1	17.9 ± 1.1
U3A3Z	18.4 ± 1.4	25.4 ± 4.3

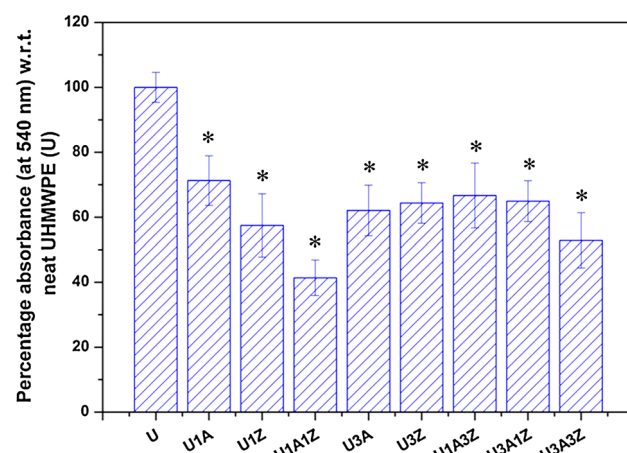


Fig. 13. Analysis of relative *S. aureus* viability showing the bactericidal property of various UHMWPE-Ag-ZnO biopolymeric biocomposites. The statistical analysis is reported by using Student's *t* test with >95% confidence level ( $p < 0.05$ ). \*The viability of *S. aureus* is significantly different from that on neat UHMWPE (U) ( $p < 0.002$ ).

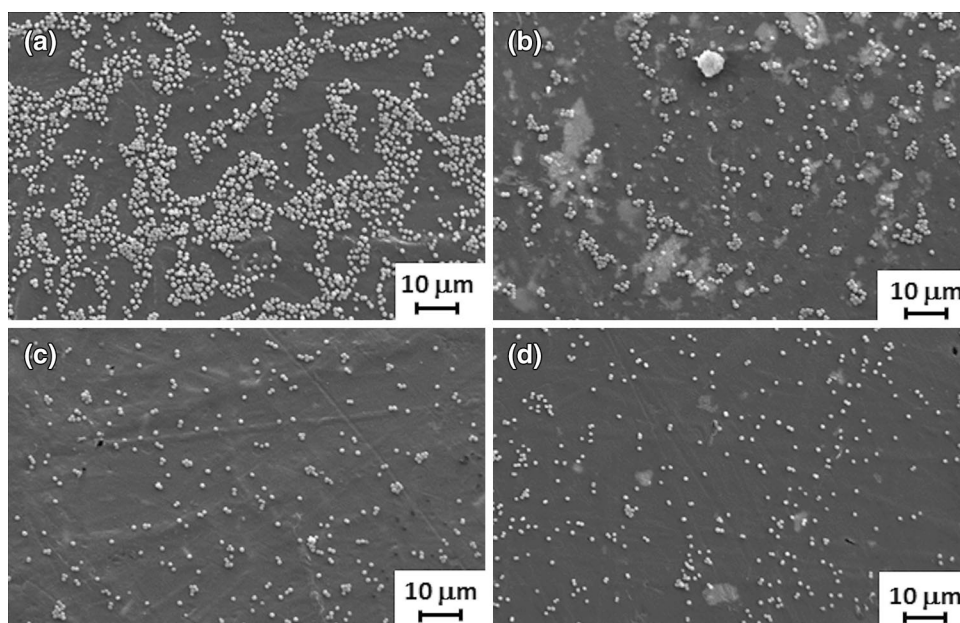


Fig. 12. SEM imaging of bacteria grown on the samples incubated for 8 h at 37°C. (a) U, (b) U3A, (c) U3Z, and (d) U3A3Z.

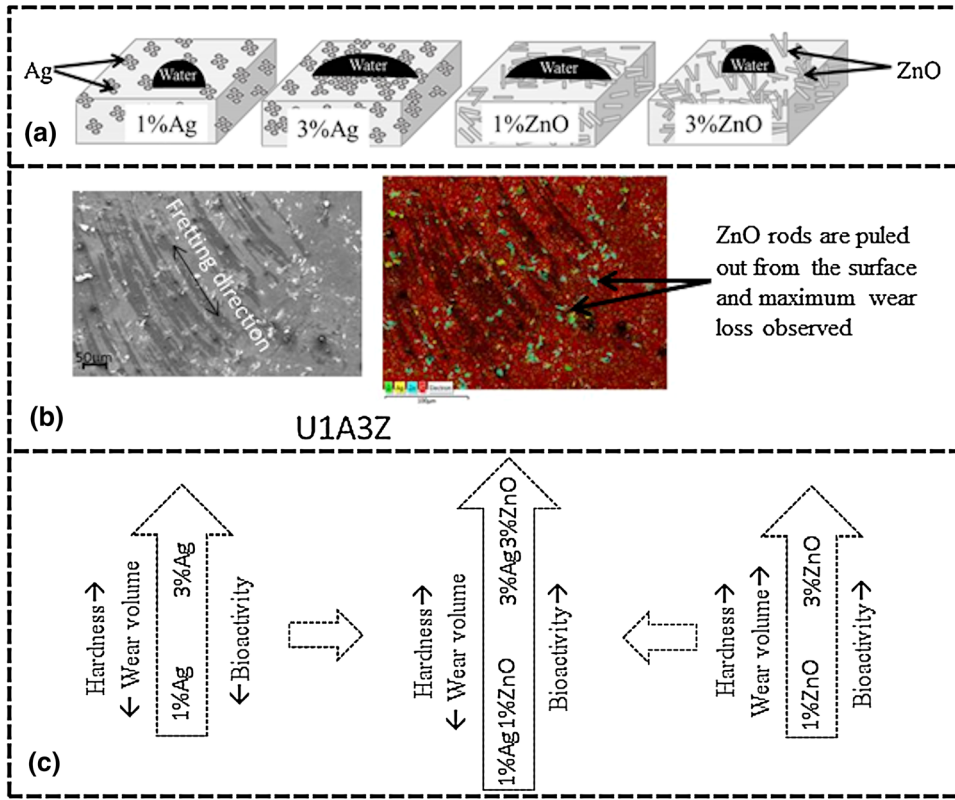


Fig. 14. Effect of Ag and ZnO reinforcement on the overall properties of the composite: (a) schematic to show how the concentration of silver and ZnO affects the wettability of the sample. (b) Elemental mapping of U1A3Z sample showing the presence of ZnO on the surface of U1A3Z sample (which has shown highest wear volume at 5/10 N load). (c) Summary of hardness, wear volume and bioactivity of Ag and ZnO reinforcement in the UHMWPE biopolymer composite (the length of arrows qualitatively indicates the trend of change).

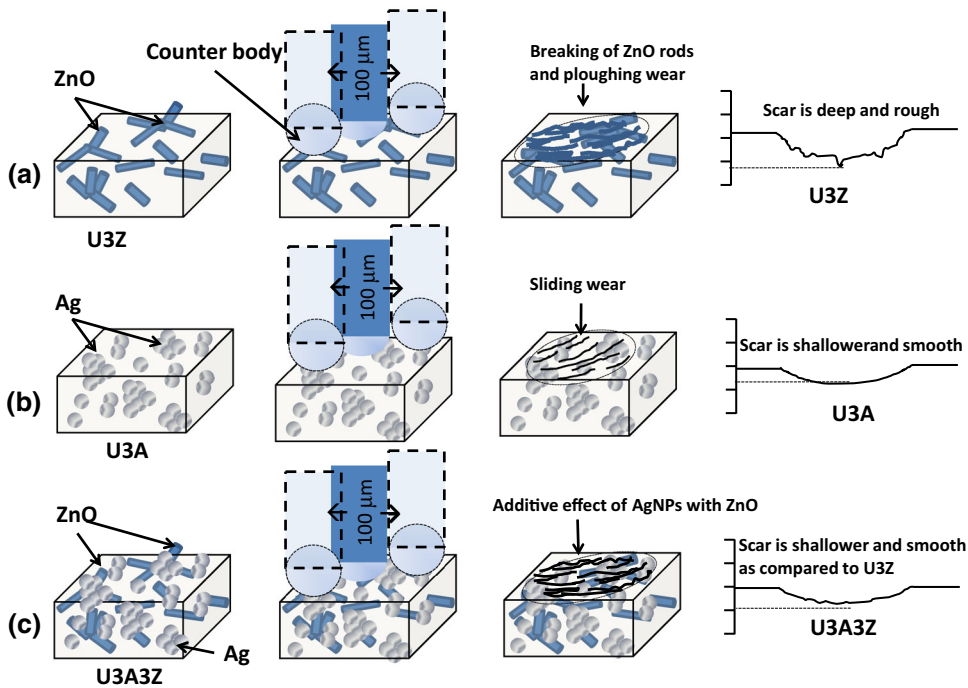


Fig. 15. Schematic representation of the fretting wear mechanism on the surface of different samples: (a) on U3Z which shows that the breaking of ZnO rods on the polymer surface changes the mechanism to ploughing, resulting in an increase in the wear loss and also the rough surfaces, (b) on U3A samples which shows that Ag NPs changes the wear mechanism to sliding wear and only slipping of the counter body occurs and wear loss is at a minimum, whereas (c) on U3A3Z which shows that Ag NPs fills the voids created by ZnO and lowers the wear volume hence showing the synergistic effect of Ag NPs with ZnO rods.

## CONCLUSION

Compression molding was successfully carried out for the preparation of Ag-/ZnO-reinforced UHMWPE samples. Phase characterization of the dense (>98% theoretical densification) compression-molded UHMWPE-ZnO-Ag samples elicited the retention of starting phases after the processing. Both Ag and ZnO reinforcement showed enhanced hardness (20.4% and 42.0%, respectively), while rendering enhanced the bioactivity quantified by the percent fraction of apatite from x-ray diffraction. A direct relationship between the polar fraction of the surface energy and consequent apatite precipitation was observed, which indicates the potential in controlling the cellular response by manipulating the material composition. It was noticed that Ag enhanced the mechanical and tribological properties, whereas ZnO contributed by enhancing the biological properties. Sample U3A3Z shows the maximum hardness, i.e.  $53.4 \pm 3.4$  MPa (~26% increase) as compared to the neat UHMWPE (U) sample with hardness of  $39.2 \pm 2.9$  MPa. Samples U1A and U3A exhibited the lowest wear volume (1.8 and 2.2 times lower, respectively), whereas samples U3Z and U1A3Z have shown the maximum wear loss (1.12 and 2.24 times higher, respectively). From the MTT assay, it was observed that *S. aureus* reduces viability by ~28.7% in the case of U1A, and with U1Z it reduces by ~42.5% than that of the control. However, such viability reduction is ~58.6% in the case of U1A1Z and ~47.1% in U3A3Z, which exhibits a synergistic role of Ag and ZnO addition in enhancing the bactericidal property in UHMWPE-Ag-ZnO biopolymer nanocomposites. Interestingly, an additive effect of Ag and ZnO (at U1A1Z and U3A3Z) elicits lower wear loss (compared to the U-Z combination) and enhanced bioactivity (compared to the U-A combination) and best anti-bacterial property. Thus, an engineered reinforcement of Ag and ZnO in UHMWPE (U1A1Z and U3A3Z) shows potential application of the UHMWPE-Ag-ZnO biopolymer nanocomposite as an articulating surface in total joint replacements.

## ACKNOWLEDGEMENTS

The authors thank MHRD, Govt. of India, for providing a grant towards the purchase of a contact angle goniometer, and DBT, Govt. of India, towards the establishment of a cell culture facility.

## REFERENCES

1. R.B. Waterhouse, *Wear* 29, 337 (1974).
2. R.B. Waterhouse, *Wear* 100, 107 (1984).
3. E. Ebramzadeh, F. Billi, S.N. Sangiorgio, S. Mattes, W. Schmoelz, and L. Dorr, *J. Biomech. Eng.* 127, 357 (2005).
4. J.A. Davidson, R.A. Poggie, and A.K. Mishra, *Biomed. Mater. Eng.* 4, 213 (1994).
5. P.L. Hurricks, *Wear* 15, 389 (1970).
6. Y. Berthier, L. Vincent, and M. Godet, *Tribol. Int.* 22, 235 (1989).
7. Q. Wang, D. Zhang, and S. Ge, *J. Eng. Tribol.* 221 (3), 307 (2007).
8. A.K. Patel, P. Trivedi, and K. Balani, *J. NanoSci. NanoEng. Appl.* 4, 1 (2014).
9. A. Gupta, G. Tripathi, B. Basu, and K. Balani, *Journal of Minerals, Metals, and Materials (JOM)* 64, 506 (2012).
10. D. Xiong and S. Ge, *Wear* 250, 242 (2001).
11. M. Mirghany and Z.M. Jin, *Proc. Inst. Mech. Eng. H* 218, 41 (2004).
12. K. Plumlee and C.J. Schwartz, *Wear* 267, 710–717 (2009).
13. D. Xiong, J. Lin, D. Fan, and Z. Jin, *J. Mater. Sci.* 18, 2131–2135 (2007).
14. S. Ge, S. Wang, and X. Huang, *Wear* 267, 770 (2009).
15. Q.J. Xue and Q.H. Wang, *Wear* 213, 54 (1997).
16. Y. Xue, W. Wu, O. Jacobs, and B. Schädel, *PolymerTesting* 25, 221 (2006).
17. A. Lucas, J.D. Ambrosio, H. Otaguro, L.C. Costa, and J.A.M. Agnelli, *Wear* 270, 576 (2011).
18. N. Reina, C. Delaunay, P. Chiron, N. Ramdane, and M. Hamadouche, *Orthop. Traumatol* 99, 551–561 (2013).
19. L. Juan, Z. Zhimin, M. Anchun, L. Lei, and Z. Jingchao, *Int. J. Nanomed.* 5, 261–267 (2010).
20. T. Jansson, Z.J. Clare-Salzler, T.D. Zaveri, S. Mehta, N.V. Dolgova, B.H. Chu, F. Ren, and B.G. Keselowsky, *J. Nanosci. Nanotechnol.* 12, 1–7 (2012).
21. K.J. Bozic and M.D. Ries, *J. Bone Joint Surgery Am.* 87, 1746–1751 (2005).
22. M.K. Steven, *The UHMWPE Handbook Ultra-High Molecular WeightPoly-ethylene in Total Joint Replacement London* (Amsterdam: ElsevierAcademic Press, 2004).
23. R.K. Sharma and K. Balani, *J. Phys. D Appl. Phys.* 47, 345301 (2014).
24. A. Gupta, G. Tripathi, D. Lahiri, and K. Balani, *J. Mater. Sci. Technol.* 29, 514 (2013).
25. C. Liu, X. Yang, H. Yuan, Z. Zhou, and D. Xiao, *Sensors* 7, 708 (2007).
26. Z.H. Ibupoto, K. Khun, M. Eriksson, M. AlSalhi, M. Atif, A. Ansari, and M. Willander, *Materials* 6, 3584 (2013).
27. A.K. Patel and K. Balani, *Mater. Sci. Eng., C* 46, 504 (2015).
28. K. Sikdar, S. Shekhar, and K. Balani, *Wear* 318, 177 (2014).
29. M.A.F. Afzal, P. Kesarwani, K.M. Reddy, S. Kalmodia, B. Basu, and K. Balani, *Mater. Sci. Eng., C* 32, 1164 (2012).
30. S. Kalmodia, S. Goenka, T. Laha, D. Lahiri, B. Basu, and K. Balani, *Mater. Sci. Eng. C* 30, 1162 (2010).
31. K. Herkendell, V.R. Shukla, A.K. Patel, and K. Balani, *Mater. Sci. Eng. C* 34, 455 (2014).
32. M.A.F. Afzal, S. Kalmodia, P. Kesarwani, B. Basu, and K. Balani, *J. Biomater. Appl.* 27, 967 (2013).
33. N. Padmavathy and R. Vijayaraghavan, *Sci. Technol. Adv. Mater.* 9, 035004 (2008) (7 pp).